

Formation of galactic bulges from the cold gas filaments in high-redshift dark matter halos

Masafumi Noguchi¹★

¹*Astronomical Institute, Tohoku University, 6-3, Aramaki, Aoba-ku, Sendai, Miyagi, 980-8578, Japan*

Accepted XXX. Received YYY; in original form ZZZ

ABSTRACT

Formation process(es) of galactic bulges are not yet clarified although several mechanisms have been proposed. In a previous study, we suggested one possibility that galactic bulges have been formed from the cold gas inflowing through surrounding hot halo gas in massive dark matter halos at high redshifts. It was shown that this scenario leads to the bulge-to-total stellar mass ratio increasing with the galaxy mass, in agreement with the well-known observed trend. We here indicate that it also reproduces recent observational results that the mean stellar age of the bulge increases with the galaxy mass while the age gradient across the bulge decreases. We infer that this formation path applies mainly to high-mass galaxies and the bulges in lower-mass galaxies have different origins such as secular formation from the disc material.

Key words: galaxies: bulges – galaxies: formation – galaxies: structure – galaxies: high-redshift

1 INTRODUCTION

Assembly of galaxies in the early universe is a matter of intense debate in current astrophysics. Among others, the formation of bulges is a key ingredient which brought about the morphological diversity of the present-day disc galaxies. Despite much effort in clarifying the bulge formation process from both observational and theoretical perspectives, we are still far from satisfactory understanding of this important piece of galaxy formation. Complex structures and kinematics of galactic bulges, especially the dichotomization into classical and pseudo bulges, suggest contribution of several mechanisms in their formation process. (Kormendy & Kennicutt 2004). Classical bulges are usually linked to early formation by direct collapse (Larson 1976; Zolotov et al. 2015) and/or minor galaxy mergers (Hopkins et al. 2009). Pseudo bulges are often alleged to be the product of the secular formation processes from the disc material, such as gas infall induced by galactic bars (e.g. Athanassoula 1992), the bending instability of the bars themselves (e.g. Raha et al. 1991), and inward migration of massive clumps formed in gas-rich young galactic discs (e.g. Noguchi 1998, 1999; Inoue & Saitoh 2012; Bournaud, Duc & Emsellem 2008).

Any consistent theory of bulge formation must explain the observed properties of other galactic components in the same framework. In seeking such a picture, we are working on the galaxy evolution model based on the cold accretion picture for gas accretion onto forming galaxies (e.g. Fardal et al. 2001; Keres et al. 2005; Dekel & Birnboim 2006). Noguchi (2020) suggested a new possibility that the bulge formation is fueled by the cold gas streams characteristic of the halo gas in massive galaxies at high redshifts. It was found that this picture can reproduce the observed trend that the mass fraction of the bulge relative to total stellar mass of the

galaxy increases with the galaxy mass. We here report that the same model can also explain the observed age structures of galactic bulges, namely the mass dependence of the mean stellar age and the age difference within the bulge region.

2 MODELS

The cold accretion theory has been proposed on the basis of realistic simulations for thermal and hydrodynamical evolution of the primordial gas in the cold dark matter universe (e.g. Fardal et al. 2001; Birnboim & Dekel 2003; Keres et al. 2005; Dekel & Birnboim 2006; Ocvirk, Pichon & Teyssier 2008; van de Voort & Schaye 2012; Nelson et al. 2013). It states that the intergalactic gas flows into the hierarchically growing dark matter halos in unheated state and fuels the forming galaxies except in the most massive halos in recent cosmological epochs, where the cooling flow of the shock heated halo gas prevails. This picture represents a major modification to the long-standing paradigm which argues that the heating by shock waves is the universal behaviour of the gas that enters growing dark matter halos (e.g. Rees & Ostriker 1977). This new scenario provides possible solutions to several observations unexplained in the shock-heating theory, including the existence of abundant luminous galaxies at high redshifts and very red colors (and therefore complete quenching of star formation) of present massive elliptical galaxies. (e.g. Cattaneo et al. 2006; Dekel et al. 2009).

Recently, the application of this scenario was extended to subgalactic scales. Noguchi (2020) examined the morphological buildup of disc galaxies under the cold accretion while Noguchi (2018) tried to explain the chemical bimodality observed in the Milky Way disc stars (e.g. Adibekyan et al. 2012; Haywood et al. 2016; Queiroz et al. 2020). Especially, Noguchi (2020) succeeded in reproducing the structural variation of disc galaxies as a function of the galaxy mass

★ E-mail: noguchi@astr.tohoku.ac.jp (MN)

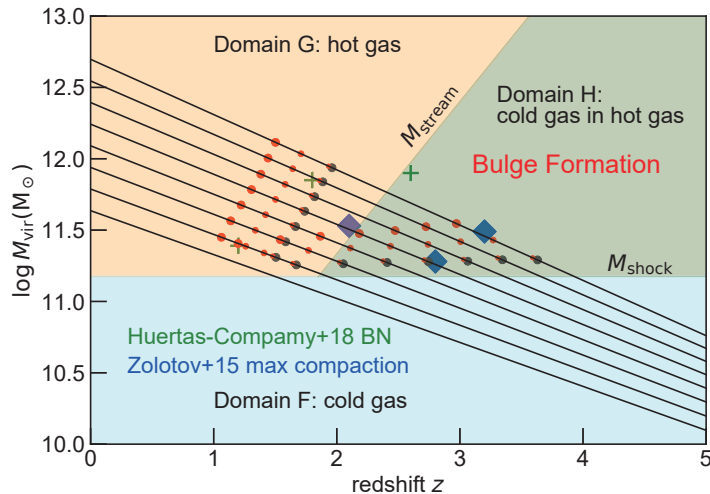


Figure 1. Evolution of the virial mass is indicated by solid lines for eight models analyzed in the present study overlaid on the three domains for the different gas states. Black circles on each evolution path indicate the two epochs between which the cold gas in Domain H arrives at the disc plane. Red circles indicate, in increasing size, the times $t_{\text{arr}} + t_{\text{dyn}}$, $t_{\text{arr}} + 10t_{\text{dyn}}$, and $t_{\text{arr}} + 20t_{\text{dyn}}$. Here, $t_{\text{dyn}} \equiv (GM_{\text{gal}}/R_{\text{gal}})^{1/2}$, where the galaxy radius is set to be $R_{\text{gal}} = 0.1R_{\text{vir}}$ considering the high spin parameter ~ 0.1 at high redshift (Danovich et al. 2015) and the galaxy mass M_{gal} includes all stars and the portion of dark matter within the galaxy radius. The peak masses for the blue nuggets observed by Huertas-Compamy et al. (2018) for three different redshifts are shown by green crosses, whereas the blue diamonds are the maximum compaction in three galaxies in VELA simulation by Zolotov et al. (2015). The virial masses for the observed BNs are derived by using the stellar-to-halo mass ratio (SHMR) by Rodríguez-Puebla et al. (2017) for the corresponding redshifts. The virial masses for the simulated galaxies are extrapolated along the expected evolutionary tracks (black lines) from the cited values at $z = 2$.

that is revealed by the photometric decomposition of stellar contents into thin and thick discs and bulges (e.g. Yoachim & Dalcanton 2006; Comeron et al. 2014). Examinations in the present work are based on the same evolution model as employed in Noguchi (2020), but we here concentrate on the age structures of the bulges and compare the model with the currently available observational data.

The cold accretion theory which underlies the present study predicts three different regimes for the properties of the gas distributed in the dark matter halos depending on the virial mass and the redshift (e.g. Dekel & Birnboim 2006; Ocvirk, Pichon & Teyssier 2008). It introduces two characteristic mass scales: M_{shock} above which the halo gas develops a stable shock that heats the gas nearly to the virial temperature and M_{stream} below which part of the halo gas remains cold and is confined into narrow filaments that thread the smoothly distributed shock-heated gas. The latter mass scale is valid only for high redshifts.

These mass scales demarcate three different regions as depicted in Fig. 1. The halo gas in Domain F is unheated and expected to accrete in free-fall to the inner region (the disc plane). In domain G, the gas heated to the virial temperature attains near hydrostatic equilibrium in the halo gravitational field and the radiative cooling induces cooling flow to the center with the cooling timescale. The gas behaviour is not so clear in Domain H, where cold gas streams coexist with the surrounding shock-heated hot gas. They may behave independently and accrete with their own timescales or they may interact with each other leading to modification of accretion timescales. Because no detailed information is available, we assume that the cold and hot gases in Domain H accrete with the free-fall time and the radiative cooling time, respectively.

In Noguchi (2020), the one-to-one correspondence was assumed between the gas components in this diagram and the three galactic mass components of disc galaxies. Namely, the cold gas in Domain

F produces thick discs, and thin discs are formed from the hot gas in Domain G. This part of correspondence is supported from the chemical point of view because it gives a satisfactory reproduction of the stellar abundance distribution for the Milky Way thin and thick discs (Noguchi 2018). The hot gas in Domain H is assumed to result into additional thin discs, while the cold gas produces bulges. This whole hypothesis can reproduce the observed variation in the mass ratios of thin discs, thick discs, and bulges with the galaxy mass as shown in Noguchi (2020). The cosmological simulation of Brooks et al. (2009) also suggests the correspondence between the gas properties and the resultant galactic components similar to the one assumed in Noguchi (2020).

The existence of surrounding hot gas, characteristic of Domain H, may indeed provide favourable condition for bulge formation from the embedded cold gas. Bieri et al. (2016) have shown that the external pressure resulting from AGN feedback triggers active star formation in galactic discs by promoting the formation of massive clumps in the destabilized discs. The simulation by Du et al. (2019) may provide another relevant result. It shows that the ram pressure of the hot gas around massive galaxies exerted on inplunging dwarf galaxies confines their metal-rich gas produced by supernovae and stellar winds, leading to subsequent star formation. The hot halo gas in Domain H thus may help clumps formed in the cold gas streams survive until they create centrally concentrated stellar systems for example by radial migration. Based on these considerations, we adopt the same correspondence hypothesis as in Noguchi (2020) in this study.

The locations of the borders of three domains shown in Fig. 1 actually depend on the detailed physical state (e.g., metallicity, temperature) of the gas infalling into dark matter halos which is only poorly constrained by the observation (e.g. Dekel & Birnboim 2006; Ocvirk, Pichon & Teyssier 2008). We use the same configuration as

adopted in [Noguchi \(2020\)](#) because it leads to good reproduction of the observed mass fractions of the thin discs, thick discs, and bulges as a function of the galaxy mass observed by [Yoachim & Dalcanton \(2006\)](#) and [Comeron et al. \(2014\)](#). To be specific, we assume that $M_{\text{shock}} = 1.5 \times 10^{11} M_{\odot}$ and $\log M_{\text{stream}} = 9.2 + 1.067z$. Both M_{shock} and M_{stream} are smaller than those indicated in Fig. 7 of [Dekel & Birnboim \(2006\)](#) but closer to the [Keres et al. \(2005\)](#) shock mass and the [Ocvirk, Pichon & Teyssier \(2008\)](#) stream mass.

The model used here treats a disc galaxy as a three-component stellar system comprising a thin disc, a thick disc and a bulge embedded in a dark matter halo that grows in mass as specified by the hierarchical mergers of dark matter halos. Following [Wechsler et al. \(2002\)](#), the growth of the virial mass is given by

$$M_{\text{vir}} = M_{\text{vir},0} e^{-2z/(1+z_c)} \quad (1)$$

where $M_{\text{vir},0}$ is the present halo mass and z_c is the collapse redshift explained below. The NFW density profile is assumed with the evolving concentration parameter

$$c(z) = \min \left[K \frac{1+z_c}{1+z}, K \right] \quad (2)$$

with $K = 3.7$ ([Bullock et al. 2001](#)). z_c is calculated once the present concentration $c(0)$ is specified. We assume following [Maccio, Dutton & van den Bosch \(2008\)](#) that

$$\log c(0) = 0.971 - 0.094 \log(M_{\text{vir},0}/[10^{12} h^{-1} M_{\odot}]) \quad (3)$$

Growth of each component is driven by the accretion of gas from the halo, the timescale of which is determined by the cold accretion theory. Namely, the gas newly added to the halo in Domain F is assumed to accrete with the free-fall time (dynamical time) defined by $(GM_{\text{vir}}/R_{\text{vir}})^{1/2}$ at that moment, where R_{vir} is the virial radius. The accretion timescale in Domain G is the radiative cooling time of the collisionally excited gas with the halo virial temperature and metallicity $Z = 0.01Z_{\odot}$, calculated from [Sutherland & Dopita \(1993\)](#). The gas density is taken to be the halo density at the virial radius multiplied by the cosmic baryon fraction of 0.17, assuming the NFW density profile. The cold gas which occupies half the newly added gas in mass in Domain H is assumed to accrete with the free-fall time whereas the residual hot gas accretes with the radiative cooling time. The gas mass added is assumed to be the increase of the halo total mass multiplied by the cosmic baryon fraction. These specifications determines the mass accretion rate for each gas component completely.

We do not consider the internal structure (i.e., the density distribution) of each stellar component. Each component is characterized only by its mass and we calculate its time variation under the gas accretion from the halo. Actually, a significant part of the accreted gas is expected to escape from the galaxy due to feedback from star formation events such as supernova explosions especially for low mass galaxies. The fraction of this expelled gas is assumed to be proportional to the inverse of the halo virial velocity at the accretion time and the mass of the expelled gas is adjusted so that the stellar-to-virial mass ratio at present agrees with the observed one (Fig.5 of [Rodríguez-Puebla et al. \(2015\)](#) for blue galaxies). In this study, we assume that the cold gas contained in the halo in Domain H is turned into bulge stars immediately when it accretes onto the disc plane (the disc arrival time, t_{arr}). This is likely to be oversimplification and the possible effect of delay is discussed in section 4. Another caveat is that it is not clear if galaxies at high redshifts have a disc. [Dekel et al.](#)

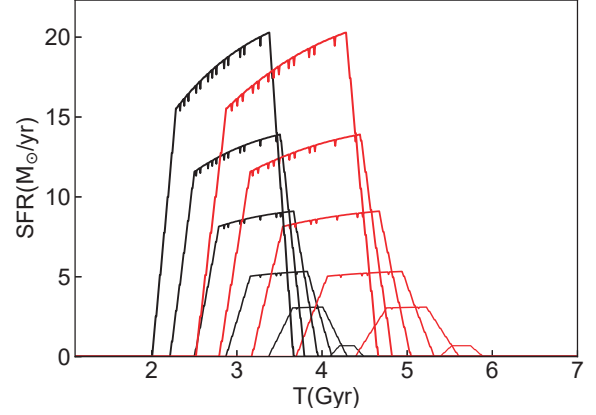


Figure 2. Star formation rate for the bulge component as a function of time, with thicker black lines indicating models with larger virial masses at present. Plotted values are running means with the width of 0.28 Gyr. Tiny spikes are caused by the numerical method used in the evolution model and do not affect our conclusions. Red lines indicate the star formation history for which delay of twenty dynamical times is taken into account.

(2020) argue that thin discs cannot develop below the critical stellar mass of $\sim 10^{10} M_{\odot}$ due to frequent mergers. The observation by [Zhang et al. \(2019\)](#) suggests that galaxies in this mass range tend to be not discy but prolate at $z \sim 2$. The present model cannot discuss the shape evolution of galaxies by construction and the disc envisaged in the present study should not be taken literally but should be more appropriately regarded as the inner part where most stars are distributed.

Bulge formation in the present scenario is restricted to relatively massive galaxies. We run a series of models with the present halo virial masses in the range $4.33 \times 10^{11} M_{\odot} \leq M_{\text{vir},0} \leq 4.98 \times 10^{12} M_{\odot}$. The evolution of more massive galaxies is likely to be dominated by mergers that could turn those galaxies into elliptical galaxies. The tracks of calculated models are shown in Fig.1. The least massive model (and models less massive than this) does not enter Domain H so that no bulge component is formed.

3 RESULTS

Fig.2 illustrates the star formation history for each model. It is seen that more massive models form bulges earlier than less massive ones and the bulge formation in those models spans longer periods in time. These trends are illustrated in a different form in Fig.1, where two black circles on each evolutionary track indicate the redshifts at which the cold accretion originating in Domain H reaches to the disc plane first and last. This mass dependence of bulge formation history is quantified and compared with observations later.

Fig.3 shows the mass fraction of the bulge as a function of the total stellar mass of the galaxy at the present epoch. We compare the model with three sets of the observation. The sample of [Gadotti \(2009\)](#) comprises nearly face-on galaxies extracted from the Sloan Digital Sky Survey. [Weinzirl et al. \(2009\)](#) decomposed H-band images of S0/a-Sm galaxies in the Ohio State University Bright Spiral Galaxy Survey ([Eskridge et al. 2002](#)). Finally, [Breda & Papaderos \(2018\)](#) analyzed 135 late-type galaxies from the CALIFA survey ([Sanchez et al. 2012, 2016](#)). The observed bulge masses likely suffer from large uncertainties as guessed from this figure. Neverthe-

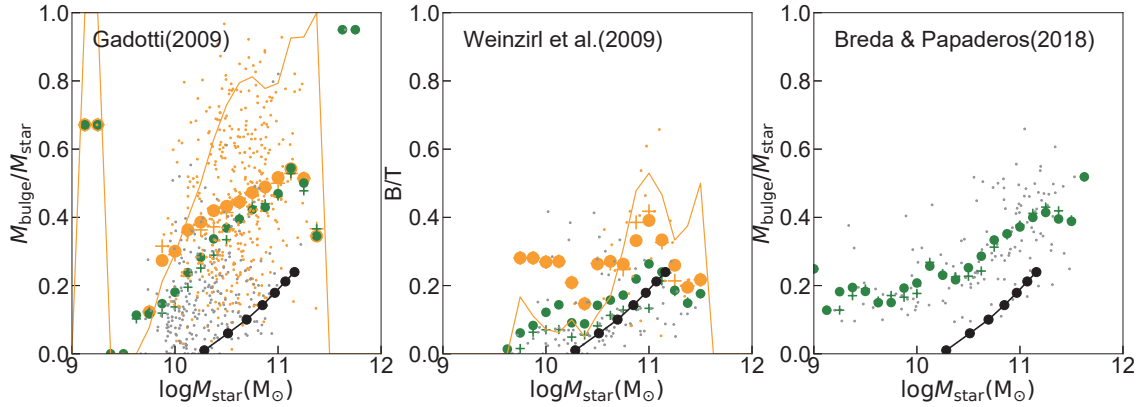


Figure 3. Model bulge fractions compared with three sets of observations. Black dots connected by solid lines are model results, whereas observational data are represented by small dots. Green circles and pluses indicate, respectively, the running mean and median in the mass bin having the width of 0.25 dex and moved by every 0.125 dex in the galaxy total stellar mass. In the left and central panels, orange symbols denote means and medians only for classical bulges (orange small dots) defined to have the Sérsic index larger than 2 in i-band and H-band, respectively. The orange lines indicate the number fraction of classic bulges in each mass bin. [Breda & Papaderos \(2018\)](#) do not derive the Sérsic index and no classification of bulges is possible.

less, the three different analyses consistently indicate the increase in bulge mass fraction with the total stellar mass. The model reproduces this qualitative trend. Model values agree well with the result of [Weinzirl et al. \(2009\)](#) but about half the values reported by [Gadotti \(2009\)](#) and [Breda & Papaderos \(2018\)](#). We discuss possible reasons for this discrepancy later.

Fig.4 summarizes the age structures of the model bulges. The mean stellar age plotted in the upper panel increases with the total stellar mass in qualitative agreement with the observation by [Breda & Papaderos \(2018\)](#). However, the model dependence (black circles) is shallower than the observed one and the discrepancy increases toward lower galaxy masses. We discuss later the effect of including possible delay in the bulge star formation. The present model predicts the lower mass limit for bulge formation originating in Domain H around $M_{\text{star}} \sim 10^{10} M_{\odot}$. We discuss later possible different origins for bulges in lower mass galaxies plotted in Fig.4.

The age difference plotted in the bottom panel is simply the time at which the bulge star formation starts minus the time at which it ends. Because the gas that accretes to the disc plane later ends up at a larger distance from the galactic center, the age difference thus defined essentially corresponds to the ‘age gradient within the bulge radius’ shown in Fig.2 of [Breda et al. \(2020\)](#). It should be noted that the ‘gradient’ given in [Breda et al. \(2020\)](#) is not the age difference per unit length but the difference between the outer and inner edges of the bulge. Reflecting the inside-out nature of gas accretion, all the models produce negative gradients. Furthermore the absolute value of the gradient increases with the galaxy mass. Over the mass range for which the model produces bulges, the model values are in good agreement with the observed ones.

4 DISCUSSION AND CONCLUSIONS

We have shown that the present model which is based on the cold accretion scenario for galactic gas accretion reproduces the observed bulge properties despite its idealized nature although some discrepancy remains. In alliance with its success in explaining the chemical bimodality in the Milky Way disc ([Noguchi 2018](#)) and the

morphological variation with the galaxy mass observed for extragalaxies ([Noguchi 2020](#)), this result may be regarded to reinforce the cold accretion scenario from the viewpoint of internal structures of individual disc galaxies. Nevertheless, there are missing ingredients in the simplified approach taken here. We touch upon these unresolved issues in the following.

In addition to the bulge mass fraction, the bulge size is also known to increase with the galaxy total stellar mass (e.g. [Gadotti 2009](#)). Although the present model cannot determine the bulge size because of its one-zone nature, it may be instructive to make rough estimate for the expected size from the virial radius R_{vir} and the spin parameter λ of the dark matter halo. The size calculated as $r_{\text{bulge}} = \lambda R_{\text{vir}}$ at the bulge formation epoch is $2 \sim 3$ kpc assuming $\lambda = 0.03$, which is similar to the observed sizes for the most massive galaxies but depends little on the galaxy mass for the calculated mass range. This is because the lower-mass galaxies experience bulge formation later than the higher-mass galaxies so that the virial radius at the bulge formation epoch as defined in this study is nearly constant with the galaxy mass.

We assumed that the cold gas in Domain H is turned into stars upon its arrival at the disc plane. This assumption may be oversimplified. It is conceivable that the cold gas streams contain gas clumps and after disc arrival individual clumps are transported inward due to violent disc instability (VDI) before star formation occurs in them (or while making stars en route to the galactic center). Clump formation within the cold gas filaments due to gravitational instability is suggested by [Mandelker et al. \(2018\)](#) in relation to globular cluster formation. Many cosmological simulations also reveal gas clumps in those filaments (e.g. [Keres et al. 2005](#); [Dekel & Birnboim 2006](#); [Ocvirk, Pichon & Teyssier 2008](#); [van de Voort & Schaye 2012](#); [Nelson et al. 2013](#)), part of which are brought in to forming galactic disks ([Dekel, Sari & Ceverino 2009](#)). Radial migration timescale due to VDI is estimated to be of the order of ten times the dynamical time ([Dekel & Burkert 2014](#)). Red circles in Fig.1 and Fig.4 illustrate how this delay affects the star formation epochs and age structures of the bulges. We see that the inclusion of star formation delay improves the agreement with the observation (especially bulge ages) with the delay time of ten times the dynamical

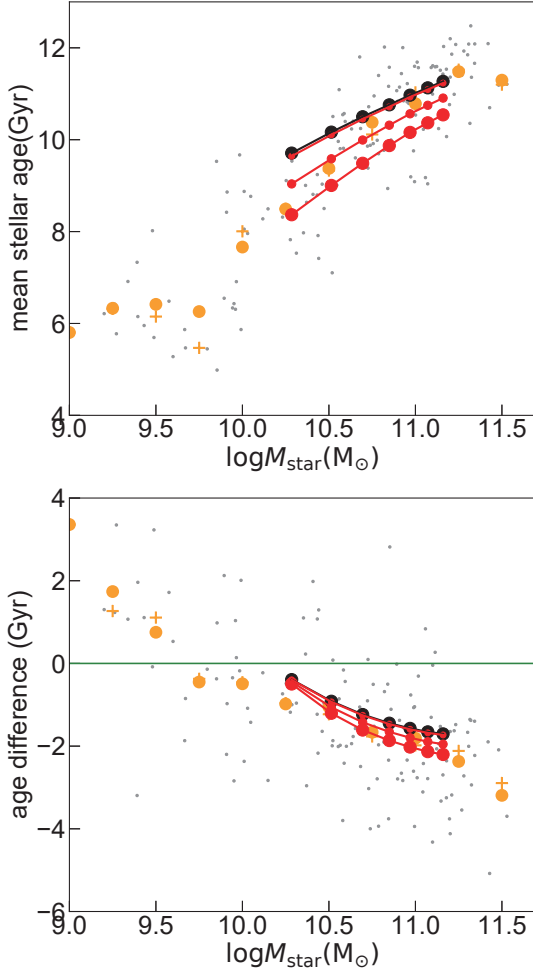


Figure 4. The mass-weighted mean stellar age of the bulge (upper panel) and the age difference over the bulge radius (bottom panel) are compared with the observational data of [Breda & Papaderos \(2018\)](#) and [Breda et al. \(2020\)](#), respectively. Each observed value is plotted with gray. Orange circles and pluses indicate the mean and median in each mass bin with the width of 0.25 dex. No star formation delay is taken into account for black circles. Red circles indicate, in increasing size, the results with the delay time, t_{dyn} , $10t_{\text{dyn}}$, and $20t_{\text{dyn}}$.

ical time giving the best fit. Influence of delay is larger for smaller galaxies because of longer migration times, resulting to significantly younger bulge ages than the fiducial case (black circles in Fig.4).

Bulge formation in the present study may be related to the compaction and blue nuggets (BNs) reported in the cosmological simulation by [Zolotov et al. \(2015\)](#). Fig.1 plots the simulated compaction events on the $z - M_{\text{vir}}$ plane. They are located in the bulge formation region in the present model bordered by black and red circles. The peak masses for the BNs observed by [Huertas-Company et al. \(2018\)](#) in different redshift ranges also fall on the domain ex-

pected for bulge formation once a certain delay from the disc arrival is taken into account. The star forming galaxies at $z \sim 2$ observed by [Tacchella et al. \(2016\)](#) exhibit different star formation profiles depending on the stellar mass with galaxies of intermediate masses ($10^{10.1} M_{\odot} < M_{\text{star}} < 10^{10.6} M_{\odot}$) showing more centrally-concentrated profiles than either less massive or more massive galaxies. This result also seems to be in line with the present study which proposes bulge formation in the restricted mass range, $M_{\text{shock}} < M_{\text{vir}} < M_{\text{stream}}$.

The present model predicts bulge formation only above a certain threshold for the present galaxy mass around $M_{\text{star}} \sim 10^{10} M_{\odot}$. It is possible that bulge formation involves several mechanisms and those bulges in less massive galaxies are formed by different processes. One possibility is the secondary bulge formation from disc material in later cosmological epochs as mentioned in introduction. Indeed, the upper panel of Fig.4 shows a steep decrease in bulge ages below $M_{\text{star}} \sim 10^{10} M_{\odot}$ in the observation by [Breda et al. \(2020\)](#). The age gradient (the bottom panel) also turns to positive below this critical mass, suggesting a different mechanism operating other than the inside-out gas accretion from the halo. There seems to be a tendency that classical bulges inhabit massive galaxies whereas pseudo bulges are observed in less massive galaxies ([Gadotti 2009](#); [Weinzirl et al. 2009](#); [Fisher & Drory 2011](#)). This habitat segregation may make the cold-accretion driven bulge formation proposed in this study a likely candidate specific to classical bulge formation. Indeed, Fig.3 shows that the threshold mass for bulge formation in the model nearly coincides with the mass above which the classical bulges start to emerge in actual disc galaxies. If this inference is correct, part of the discrepancy between the model and observations appearing in Fig.3 may be also solved. The observed excess of the bulge mass in [Gadotti \(2009\)](#) and [Breda & Papaderos \(2018\)](#) could be contributed by secular processes. On the other hand, the bulge fraction in [Weinzirl et al. \(2009\)](#), which is actually the luminosity fraction in H-band, could be underestimated if the stellar population in the bulge is systematically older (and therefore redder) than the disc in those galaxies, which is quite likely. In either case, we need not consider that the classical and pseudo bulge formation processes occur exclusively with each other. Regarding bulge formation, the galaxy mass sequence may be a continuous sequence along which the relative importance of two (or more) bulge formation processes changes gradually.

We applied for the first time the cold-accretion driven galaxy evolution model to the currently available observational data for bulge properties in galaxies with various masses. The model, despite its highly idealized nature, can reproduce the observed behaviours at least qualitatively, although observational data are still meager and future observations are required to construct a more concrete picture for bulge formation. Especially, galaxies at $z \sim 2 - 3$ will provide wealth of information on the bulge formation because galactic bulges are thought to grow vigorously in this epoch (see Fig.1). It is interesting that [Tacchella et al. \(2016\)](#) found a sign for increasing bulge dominance for more massive galaxies in this redshift range in agreement with the theoretical result by [Noguchi \(2020\)](#). The scrutinization of internal properties of the nearby bulges such as performed by [Breda & Papaderos \(2018\)](#) and [Breda et al. \(2020\)](#) will put constraints at the present cosmological epoch, playing a complementary role with high-redshift surveys.

On the theoretical side, recent cosmological simulations start to produce disc galaxies with realistic bulge-to-disc mass ratios unlike early simulations that produced too massive bulge components (e.g. [Marinacci, Pakmor & Springel 2014](#); [Gargiulo et al. 2019](#)). [Gargiulo et al. \(2019\)](#) report that their bulges in the Auriga simulation comprise mostly in-Situ stars and merger contribution is

negligible. The work of [Brooks et al. \(2009\)](#) is pioneering in that it related different structural components of disc galaxies formed in the cosmological simulations to different modes of gas accretion, namely accretion of clumpy, shocked, and unshocked gas. Although high-resolution cosmological simulations are very expensive, such close inspection of even a small number of created galaxies will provide valuable insight into the build-up of disc galaxies free from idealization made in the present work.

ACKNOWLEDGEMENTS

We thank Iris Breda and Polychronis Papaderos for providing the observational data for galactic bulges and stimulating discussion on the bulge formation mechanisms. We also thank the anonymous referees for invaluable comments which helped improve the manuscript.

Data availability

The data underlying this article will be shared on reasonable request to the corresponding author.

REFERENCES

- Adibekyan V. Zh. et al., 2012, *A&A*, 545, 32
 Athanassoula E., 1992, *MNRAS*, 259, 328
 Bieri R. et al., 2016, *MNRAS*, 455, 4166
 Birnboim Y., Dekel A., 2003, *MNRAS*, 345, 359
 Bournaud F., Duc P.A., Emsellem E., 2008, *MNRAS*, 389, L8
 Breda I., Papaderos P., 2018, *A&A*, 614, 48
 Breda I. et al., 2020, *A&A*, 635, 177
 Brooks A.M. et al., 2009, *ApJ*, 694, 396
 Bullock J.S. et al., 2001, *MNRAS*, 321, 559
 Cattaneo A. et al., 2006, *MNRAS*, 370, 1651
 Comeron S. et al., 2014, *A&A*, 571, 58
 Danovich M. et al., 2015, *MNRAS*, 449, 2087
 Dekel A., Birnboim Y., 2006, *MNRAS*, 368, 2
 Dekel A., Burkert A., 2014, *MNRAS*, 438, 1870
 Dekel A. et al., 2009, *Nature*, 457, 451
 Dekel A. et al., 2020, *MNRAS*, 493, 4126
 Dekel A., Sari R., Ceverino D., 2009, *ApJ*, 703, 785
 Du M. et al., 2019, *ApJ*, 875, 58
 Eskridge P.B. et al., 2002, *ApJS*, 143, 73
 Fardal M. A. et al., 2001, *ApJ*, 562, 605
 Fisher D.B., Drory N., 2011, *ApJ*, 733, L47
 Gadotti D.A., 2009, *MNRAS*, 393, 1531
 Gargiulo I.D. et al., 2019, *MNRAS*, 489, 5742
 Haywood M. et al., 2009, *A&A*, 589, 66
 Hopkins P.F. et al., 2009, *ApJ*, 691, 1168
 Huertas-Company M. et al., 2018, *ApJ*, 858, 114
 Inoue S., Saitoh T.R., 2012, *MNRAS*, 422, 1902
 Keres D. et al., 2005, *MNRAS*, 363, 2
 Kormendy J., Kennicutt R.C., 2004, *ARA&A*, 42, 603
 Larson R.B., 1976, *MNRAS*, 176, 31
 Maccio A.V., Dutton A.A., van den Bosch, F.C. 2008, *MNRAS*, 391, 1940
 Mandelker N. et al., 2018, *ApJ*, 861, 148
 Marinacci F., Pakmor R., Springel V., 2014, *MNRAS*, 437, 1750
 Nelson D. et al., 2013, *MNRAS*, 429, 3353
 Noguchi M., 1998, *Nature*, 392, 253
 Noguchi M., 1999, *ApJ*, 514, 77
 Noguchi M., 2018, *Nature*, 559, 585
 Noguchi M., 2020, *MNRAS*, 494, L37
 Ocvirk P., Pichon C., Teyssier R., 2008, *MNRAS*, 390, 1326
 Queiroz A.B.A. et al., 2020, *A&A*, 638, 76
 Raha N. et al., 1991, *Nature*, 352, 411
 Rees M.J., Ostriker J.P., 1977, *MNRAS*, 179, 541
 Rodriguez-Puebla A. et al., 2015, *ApJ*, 799, 130
 Rodriguez-Puebla A. et al., 2017, *MNRAS*, 470, 651
 Sanchez S.F. et al., 2012, *A&A*, 538, 8
 Sanchez S.F. et al., 2016, *A&A*, 594, 36
 Sutherland R.S., Dopita M., 1993, *ApJS*, 88, 253
 Tacchella S. et al., 2016, *MNRAS*, 458, 242
 van de Voort F., Schaye J., 2012, *MNRAS*, 423, 2991
 Wechsler R.H. et al., 2002, *ApJ*, 568, 52
 Weinzirl T. et al., 2009, *ApJ*, 696, 411
 Yoachim P., Dalcanton J.J., 2006, *AJ*, 131, 226
 Zhang H. et al., 2019, *MNRAS*, 484, 5170
 Zolotov A. et al., 2015, *MNRAS*, 450, 2327

This paper has been typeset from a $\text{\TeX}/\text{\LaTeX}$ file prepared by the author.